

Correlations between charge radii differences of mirror nuclei and stellar observables

P. Bano ¹, S. P. Pattnaik ¹, M. Centelles ², X. Viñas ^{2,3} and T. R. Routray ^{1,*}

¹*School of Physics, Sambalpur University, Jyotivihar 768 019, India*

²*Departament de Física Quàntica i Astrofísica (FQA) and Institut de Ciències del Cosmos (ICCUB), Universitat de Barcelona (UB), Martí i Franquès 1, E-08028 Barcelona, Spain*

³*Institut Menorquí d'Estudis, Camí des Castell 28, 07702 Maó, Spain*



(Received 5 April 2023; accepted 22 June 2023; published 13 July 2023)

The correlation between the charge radii differences in mirror nuclei pairs and the neutron skin thickness has been studied with the so-called finite range simple effective interaction over a wide mass region. The so far precisely measured charge radii difference data within their experimental uncertainty ranges in the ^{34}Ar - ^{34}S , ^{36}Ca - ^{36}S , ^{38}Ca - ^{38}Ar , and ^{54}Ni - ^{54}Fe mirror pairs are used to ascertain an upper limit for the slope parameter of the nuclear symmetry energy $L \approx 100$ MeV. This limiting value of L is found to be consistent with the upper bound of the NICER PSR J0740+6620 constraint at 1σ level for the radius $R_{1.4}$ of $1.4M_{\odot}$ neutron stars. The lower bound of the NICER $R_{1.4}$ data constrains the lower limit of L to ≈ 70 MeV. Within the range for $L = 70$ – 100 MeV the tidal deformability $\Lambda^{1.4}$ constraint, which is extracted from the GW170817 event at 2σ level, and the recent PREX-2 and CREX data on the neutron skin thickness are discussed.

DOI: [10.1103/PhysRevC.108.015802](https://doi.org/10.1103/PhysRevC.108.015802)

I. INTRODUCTION

With the advent of collinear laser beam technology [1,2], the precise measurement of nuclear charge radii in the magic nuclei isotopic chains for the medium-heavy mass region ranging between $Z = 19$ to $Z = 50$ could be completed with the recent measurements of the Ni-isotopic chain ([3] and references therein). Due to this high-precision technology, the charge radii difference, ΔR_{CH} , between the two nuclei of a mirror pair can be measured accurately. The experimental determination of ΔR_{CH} of mirror pairs provides the opportunity of estimating the neutron skin thickness in nuclei, ΔR_{np} , under the isospin symmetry of the nucleon-nucleon (NN) interaction [4–11]. Taking into account the charge symmetry breaking effects, ΔR_{CH} of mirror nuclei appears to be a clean (electromagnetic) alternative method to the electroweak parity-violating asymmetry [12] and electric dipole polarizability [13–15] measurements for the estimation of the neutron skin thickness. The neutron skin ΔR_{np} in a nucleus is defined as the difference between the root-mean-square (rms) neutron and proton radii ($R_n - R_p$). Given that ΔR_{np} of neutron-rich nuclei is strongly correlated to the slope of the symmetry energy L [16–19], the knowledge of ΔR_{np} is very valuable for constraining the equation of state (EoS) of isospin-asymmetric matter. However, neutron radii of nuclei, and hence neutron skins, are more difficult to determine with high accuracy than charge radii. In mirror nuclei the measurement of the neutron radius may be bypassed if one takes into account, that under perfect charge symmetry of the NN interaction, the neutron radius of the nucleus with Z protons

and N neutrons equals the proton radius of its mirror pair with N protons and Z neutrons. Then, the neutron skin of a (Z, N) nucleus can be obtained from the charge radii of the mirror pair as $\Delta R_{np} = \Delta R_{\text{CH}} \equiv R_{\text{CH}}(N, Z) - R_{\text{CH}}(Z, N)$ [7,9]. In reality, the Coulomb interaction breaks the perfect charge symmetry and the equality between ΔR_{CH} and ΔR_{np} is weakened. It is therefore important to study the degree of correlation preserved between ΔR_{CH} and ΔR_{np} , and between ΔR_{CH} and the symmetry energy slope L .

An interesting current trend in the literature is to use the neutron skin property of finite nuclei to extract information on the L value, i.e., the pressure in pure neutron matter, and use this to study astrophysical observables under certain assumptions [7,20,21]. The measurement of the neutron skin thickness in finite nuclei has important implications for neutron star (NS) properties, such as the radius and the tidal deformability of NSs [20], and complements the gravitational wave (GW) observations [19,22–26]. Also, recent studies have pointed out the possible correlation between the mirror pair charge radii difference ΔR_{CH} and the radius of NSs [5]. But invariably the range for L extracted from the correlation of the terrestrial data and celestial observables could barely explain the PREX-2 result of $\Delta R_{np}^{208} = 0.283 \pm 0.071$ fm for the neutron skin thickness in ^{208}Pb , obtained in a model-independent way from parity violating electron scattering (PVES) measurements [27]. Moreover, the recently published CREX result of $\Delta R_{np}^{48} = 0.121 \pm 0.026(\text{exp}) \pm 0.024(\text{model})$ fm in ^{48}Ca [28] from a similar PVES experiment suggests the question of why the skin thickness in ^{48}Ca is so thin. Although this low value of the skin in ^{48}Ca has been predicted by chiral effective field theory (EFT) calculations [29,30], the PREX-2 and CREX measurements together pose a challenge

*Corresponding author: trr1@rediffmail.com

to the theoretical models for the simultaneous reproduction of both data under the present scenario of incomplete knowledge of the EoS of neutron-rich nuclear matter, as discussed in Refs. [31–33] within the energy density functional (EDF) approach. The computation of ^{208}Pb from *ab initio* theory has not been feasible before now, but combined with advances in quantum many-body techniques has predicted the neutron skin in ^{208}Pb to be $\Delta R_{np}^{208} = 0.17 \pm 0.05$ fm at 90% confidence level [34], and a value in ^{48}Ca of $\Delta R_{np}^{48} = 0.16 \pm 0.04$ fm at the same confidence level [34].

In this work, using the so-called finite range simple effective interaction (SEI) model we examine the global correlation between ΔR_{CH} and ΔR_{np} and show a linearity between them, confirming the trends previously found in Skyrme forces [4,8] and in chiral EFT calculations in the low-energy limit [6]. In former studies we have shown that SEI accurately satisfies a wide range of constraints in nuclear matter and nuclear structure [35–39]. Also SEI has been used in the astrophysical domain to derive the mass-radius relation in NSs as well as dynamical properties, such as the r -mode oscillation and spin-down features associated with NS physics [40–44]. Here, we next use the SEI model to study the experimental ΔR_{CH} data available for four mirror pairs. We find that these accurate experimental results, together with the NICER telescope data, which constrain the radius of $1.4M_{\odot}$ NSs from observations on pulsar PSR J0740+6620 [45], predict from the analysis with SEI that the symmetry energy slope L lies in a range between 70 and 100 MeV. The validity of the L range thus obtained is examined in the context of the tidal deformability constraint extracted from the GW170817 detection of gravitational waves from a binary NS merger [46], together with the results from the PREX-2 [27] and CREX [28] experiments.

II. BASIC THEORY

The SEI was introduced in Ref. [35] by Behera and collaborators. Its explicit form, for a Gaussian finite range form factor, in coordinate space is given by

$$V_{\text{eff}} = t_0(1 + x_0 P_{\sigma})\delta(\vec{r}) + \frac{t_3}{6}(1 + x_3 P_{\sigma})\left(\frac{\rho(\vec{R})}{1 + b\rho(\vec{R})}\right)^{\gamma} \delta(\vec{r}) \\ + (W + BP_{\sigma} - HP_{\tau} - MP_{\sigma}P_{\tau})e^{-r^2/\alpha^2} \\ + \text{spin-orbit part}, \quad (1)$$

where a zero-range spin-orbit (SO) interaction depending on a strength parameter W_0 is taken to deal with finite nuclei. All the parameters of the interaction, except t_0 and the SO strength W_0 , namely, α , γ , b , x_0 , x_3 , t_3 , W , B , H , and M , are fitted in nuclear matter (NM) of different types using very generic considerations obtained from the experimental/empirical conditions [35–37]. For example, the density dependence of the isovector part of the EoS is fixed from the condition that the asymmetric contribution to the nucleonic part of the energy density in charge neutral beta-stable $n + p + e + \mu$ NS-matter is the maximal one [40]. This condition determines the characteristic symmetry energy slope parameter L_C for the interaction set and predicts the density dependence of the symmetry energy which is neither very stiff nor very

soft (see in this respect Figs. 3 and 4(a) of Ref. [40]). The so-determined L_C is in the range ≈ 75 – 77 MeV for the EoSs of the Gaussian form of SEI in Eq. (1) corresponding to different γ values (different incompressibility), which is in the upper ranges for the L values predicted from the theoretical studies of dipole polarizability [14,47], skin thickness in Sn [48], *ab initio* calculation of low-density neutron EoS, and maximum mass of $2.1M_{\odot}$ for NSs [49–51]. But the recent studies such as charge exchange elastic scattering [52], charge radii difference in mirror nuclei [7], pion ratio in heavy-ion collisions [53], and the PREX-2 result on the ^{208}Pb skin [27], predict larger values for the L parameter, which are safely covered by the L_C values of SEI sets. Also the range for the symmetry energy $E_s(\rho_0)$ at saturation density ρ_0 inferred from these latter studies is larger than the ones conventionally used in the Skyrme and Gogny interactions. The SEI sets predict $E_s(\rho_0)$ in the range ≈ 35 – 36 MeV, which is in good agreement with the aforementioned experimental results and with the typical values in covariant EDFs.

The ρ_0 and $E_s(\rho_0)$ values in the mentioned range for SEI are the consequence of the parameter fitting protocol to predict the charge radii of 86 even-even nuclei and the binding energies (BEs) of 161 even-even nuclei with minimum rms deviations, which are obtained in the ranges of ≈ 0.015 fm and ≈ 1.5 MeV, respectively [36,37]. For comparing with the experimental values, the charge radii were calculated from the relation $R_{\text{CH}} = \sqrt{R_p^2 + 0.64 \text{ fm}^2}$, where R_p is the point proton radius and the factor 0.64 accounts for the finite-size correction to the point proton distribution [54]. Here, one neglects the small additional contributions to the charge radius that arise from the finite size of the neutron and from relativistic effects [55]. In SEI, for a given stiffness γ of NM, there is an optimal value of the saturation density ρ_0 for which the charge radii of the 86 even-even nuclei used in the fit exhibit the minimum rms deviation from the data [37]. Therefore, in order to have consistency with the parameters of SEI, we have computed R_{CH} for the mirror nuclei discussed in this work from the same relation given above.

The full determination of the SEI parameters for symmetric and asymmetric NM and for finite nuclei is discussed in Refs. [36–39]. The SEI is able to reasonably reproduce the microscopic trends of the EoS and the momentum dependence of the mean field in NM [56–59]. The finite nuclei are described by using the quasiloca density functional theory (QLDFT) [60,61]. To deal with pairing correlations in open-shell nuclei, we use an improved BCS approach, which takes partially into account the continuum through quasibound states by the centrifugal and Coulomb barriers and allows one to perform pairing calculations near the drip lines [62]. In the SEI model we use a zero-range density-dependent pairing interaction [63] fitted to reproduce the pairing gaps in NM predicted by the Gogny interaction [36]. An excellent agreement between the predictions for spherical nuclei using the QLDFT and the full HF or HFB results including the exchange terms at mean-field level was shown in Ref. [64]. It is also found that single-particle energies calculated with SEI are in reasonable agreement with the experiment and describe the spectrum of ^{208}Pb with comparable or better quality than other effective

TABLE I. Nuclear matter saturation properties of the SEI EoS ($\gamma = 0.42$): density ρ_0 , energy per nucleon $e(\rho_0)$, incompressibility K , effective mass m^*/m , symmetry energy $E_s(\rho_0)$, and slope L of the symmetry energy.

ρ_0 (fm $^{-3}$)	$e(\rho_0)$ (MeV)	K (MeV)	m^*/m	$E_s(\rho_0)$ (MeV)	L (MeV)
0.1584	-16	240	0.711	35.5	76.71

interactions [36]. The SEI mean field also reproduces the experimental kink in the isotopic shifts of the Pb charge radii [36], which is not predicted by other nonrelativistic models, such as Skyrme and Gogny, with an isospin-independent SO interaction. The recent study on the $1f_{5/2}$ - $2p_{3/2}$ proton level crossing and spin inversion phenomena in the Ni and Cu isotopic chains, respectively, using SEI [38,39] has shown that the SEI EoS corresponding to $\gamma = 0.42$ is able to produce the experimentally observed crossing at the right mass number. In this work we use this SEI EoS, whose parameters are given in Table I of Ref. [39] and whose NM saturation properties are reported here in Table I for ready reference. It is pertinent to note that, under the fitting protocol of the SEI parameters, we can relax the condition that determines the characteristic slope parameter value L_C and alternatively impose an arbitrary L value. The SEI interaction is flexible enough so that this change in the fitting procedure does not affect the isoscalar predictions. In the isovector sector, also the n - p effective mass splitting remains invariant. As a consequence, the BEs and rms mass radii of finite nuclei are practically unaffected by the changes of L .

III. RESULTS AND DISCUSSIONS

The correlation between the skin thickness ΔR_{np} and proton rms radii difference in the mirror pair, $\Delta R_p = [R_p(N, Z) - R_p(Z, N)]$, is examined by computing them in isotonic chains of $N = 14, 28$, and 50 , and isotopic chains of $Z = 10, 20$, and 28 , which covers nuclei from light to medium-heavy mass regions. The results are shown in the six panels of Fig. 1. In each panel the results obtained with the Skyrme SLy4 and SkM* [65] sets are also given. In panels (b), (d), and (e) for $N = 28, Z = 10$ and $Z = 20$, the chiral EFT results from Ref. [6] are also shown. Using the SEI data given in the six panels we perform a linear fit,

$$\Delta R_{np} = a \Delta R_p + b, \quad (2)$$

where the values of the coefficients a and b are

$$a = 0.881 \pm 0.036 \quad b = -0.049 \pm 0.017 \text{ fm}. \quad (3)$$

Our calculation includes Coulomb and pairing correlations. For similar values of ΔR_p , the values of ΔR_{np} are nearly the same. If we measure the proton rms radii difference in a mirror nuclei pair, then from Eqs. (2) and (3) the neutron skin of the neutron-rich partner nucleus can be at once estimated. With appropriate consideration of the Coulomb effects as well as other symmetry breaking effects, the charge radii difference in mirror pairs can be a surrogate to the weak interaction PVES

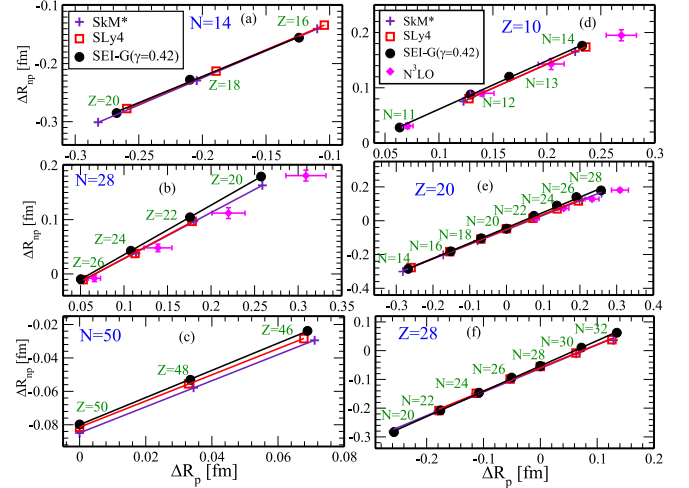


FIG. 1. Linear correlation between the neutron skin ΔR_{np} and the proton rms radii difference ΔR_p for mirror nuclei pairs shown for the SEI EoS ($\gamma = 0.42$) in the isotonic chains of (a) $N = 14$, (b) $N = 28$, and (c) $N = 50$ and isotopic chains of (d) $Z = 10$, (e) $Z = 20$, and (f) $Z = 28$. The results of SkM*, SLy4 [65] and N^3 LO [6] forces are given by symbols plus (indigo), square (red), and diamond (magenta), respectively.

experiment for skin thickness measurement. Our present study verifies the $\Delta R_p - \Delta R_{np}$ correlations reported previously in Refs. [6,8], which were obtained in the context of chiral EFT and Skyrme interactions.

Regarding the experimental information, data on the charge radii difference ΔR_{CH} in mirror pairs are available only for a few cases, within maximum neutron and proton number differences of $N - Z = 4$. We show in Table II the existing experimental data on ΔR_{CH} for the ^{34}Ar - ^{34}S , ^{36}Ca - ^{36}S , ^{38}Ca - ^{38}Ar , and ^{54}Ni - ^{54}Fe mirror pairs [4,7,9] along with the predictions computed with the SEI characteristic EoS ($L = L_C = 76.71$ MeV). These SEI results for ΔR_{CH} of the four mirror pairs are also displayed by filled black squares in the four panels of Fig. 2 together with the experimental data and the predictions of several nonrelativistic (NR) and covariant EDFs [65,66]. We see from Table II that the SEI predictions with the characteristic L_C value successfully remain well within the experimental range for the charge radii differences in the three pairs ^{34}Ar - ^{34}S , ^{36}Ca - ^{36}S , and ^{54}Ni - ^{54}Fe , and that in the ^{38}Ca - ^{38}Ar pair its ΔR_{CH} value lies just at the upper boundary of experiment. As can be realized from the results for several NR and covariant models displayed in

TABLE II. Experimental results for the charge radii difference of mirror pair nuclei and the predictions of the characteristic SEI EoS having $\gamma = 0.42$ and $L = 76.71$ MeV.

	ΔR_{CH} (fm)			
	^{34}Ar - ^{34}S	^{36}Ca - ^{36}S	^{38}Ca - ^{38}Ar	^{54}Ni - ^{54}Fe
Expt.	0.082(9)[4]	0.150(4)[7]	0.063(3)[7]	0.049(4)[9]
SEI	0.087	0.147	0.066	0.049

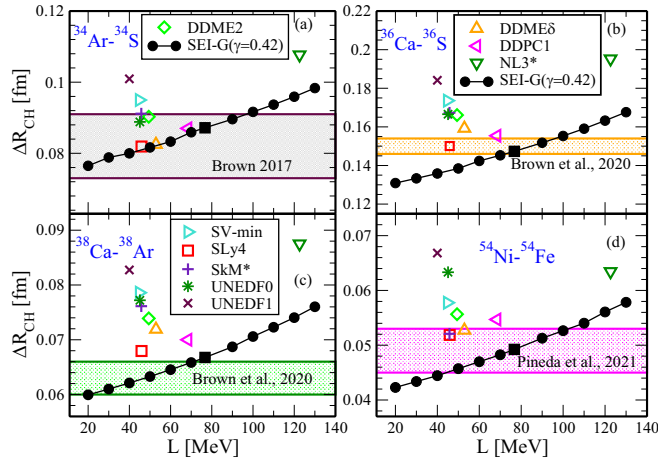


FIG. 2. ΔR_{CH} as a function of the symmetry energy slope L for the mirror pairs (a) ^{34}Ar - ^{34}S , (b) ^{36}Ca - ^{36}S , (c) ^{38}Ca - ^{38}Ar , and (d) ^{54}Ni - ^{54}Fe . The experimental results, shown in horizontal bands in each panel, are taken from Brown, 2017 [4], Brown *et al.*, 2020 [7], and Pineda *et al.*, 2021 [9]. The SEI characteristic EoS ($\gamma = 0.42$ and $L_c = 76.71$ MeV) results are shown by filled squares in the four panels, whereas the results for SEI EoSs other than $L = L_c$ are black filled circles. The results of other models are displayed by symbols as mentioned in the legends [65,66].

Fig. 2, this degree of agreement with the experimental values in these four mirror pairs seems to be difficult to satisfy by other mean field interactions.

At the mean-field level the nuclei of the mirror pairs ^{34}Ar - ^{34}S , ^{36}Ca - ^{36}S , ^{38}Ca - ^{38}Ar , and ^{54}Ni - ^{54}Fe computed with effective interactions such as the Gogny D1S and the Skyrme SLy4, SkP, and SkM* forces show a soft potential energy surface, which is compatible with a spherical shape. Dynamical quadrupole deformations can be estimated by performing beyond mean-field calculations. Consistent CHFb+5DCH calculations with the D1S interaction by Delaroche *et al.* [67] reveal that the change in the charge radius due to dynamical deformations is at most 4% in this interaction. For the mirror pairs analyzed here, it is seen [67] that the variation of the charge radius of each partner is almost identical and therefore the impact of dynamical deformation on the difference of the charge radii in a mirror pair is negligible. As far as the deformation properties of SEI are quite similar to the ones of D1S [64], we expect that beyond mean-field calculations with SEI would have a minimal effect on the charge radii differences obtained for the mirror pairs in our present spherical calculations.

The dependence of ΔR_{CH} of mirror pairs on the symmetry energy slope L has been studied within their experimental uncertainties using NR and covariant EDFs covering a wide range of L values [4,5,7,9] in order to ascertain the admissible range of values for L . To estimate the range of the slope parameter L of the EoS for which the predicted ΔR_{CH} is within the experimental error bar, we have computed ΔR_{CH} for these four mirror pairs by varying the L value of the SEI sets. As we mentioned in Sec. II, under the procedure of variation of L in SEI the binding energies and rms mass radii of nuclei remain

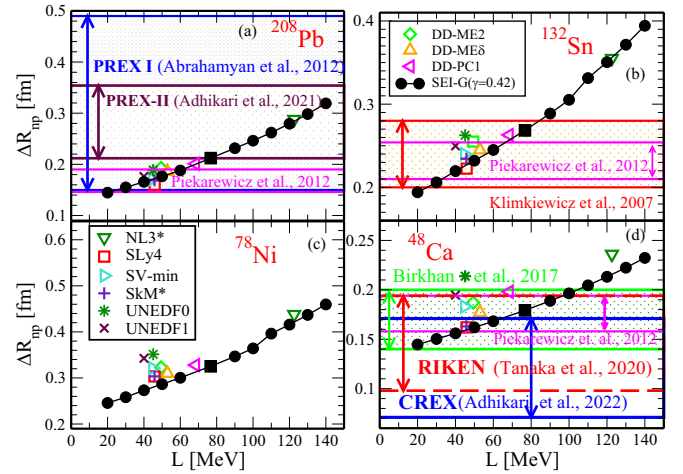


FIG. 3. Neutron skin thickness ΔR_{np} as a function of L for (a) ^{208}Pb , (b) ^{132}Sn , (c) ^{78}Ni , and (d) ^{48}Ca for SEI-G ($\gamma = 0.42$). The results extracted from theoretical analyses of the experiments are shown in horizontal bands in each panel where available and are taken from PREX I [12], PREX II [27], Piekarewicz *et al.*, 2012 [14], Klimkiewicz *et al.*, 2007 [48], Birkhan *et al.*, 2017 [68], RIKEN [69], and CREX [28].

very stable. For example, for the present nuclei in the range of variation of L from 20 to 110 MeV the BEs of $^{34,38}\text{Ar}$, ^{34}S , ^{38}Ca , ^{54}Ni , and ^{54}Fe change by less than 0.5%, and in ^{36}Ca and ^{36}S this change is $\approx 1\%$. The ΔR_{CH} values obtained under the variation of L are shown by filled black circles in the four panels of Fig. 2. The upper limit of the slope L of the symmetry energy for which the experimental error bars of these four pairs are covered by the SEI EoS comes out to be $L \approx 100$ MeV.

If we compare to the PREX-2 data on the neutron skin ΔR_{np} in ^{208}Pb , shown in panel (a) of Fig. 3, we see that SEI with its characteristic L_c predicts a neutron skin that coincides with the lower bound of the PREX-2 range. In order to reproduce the central value of 0.283 fm, the SEI requires a value of $L = 122$ MeV. In the same Fig. 3 we also display the skin thickness predicted by SEI as a function of L in ^{132}Sn , ^{78}Ni , and ^{48}Ca together with the results (except for ^{78}Ni where no data are available) obtained from the different theoretical analyses of experimental data. In the panel for ^{132}Sn , the data extracted from the pygmy dipole resonance study of [48] is shown. The very recent CREX data [28] on the ^{48}Ca skin thickness, $\Delta R_{np}^{48} = 0.121 \pm 0.026(\text{exp}) \pm 0.024(\text{model})$ fm = 0.071–0.171 fm, shown in panel (d) of this figure, demands $L \leq 65$ MeV for the SEI EoS in order to remain within the CREX uncertainty limit. However, in order to predict the central value 0.121 fm, SEI requires a very small value for L . The predictions of the SEI EoSs have a larger overlap with the results on ΔR_{np} of ^{48}Ca obtained from the dipole polarizability study [68] and from the scattering of ^{48}Ca on C at 280 MeV/nucleon [69], which are displayed in the same panel (d) of Fig. 3. The correlation between ΔR_{np} and the proton radii difference in mirror pairs, Eqs. (2) and (3), could be the yardstick to these various measurements in

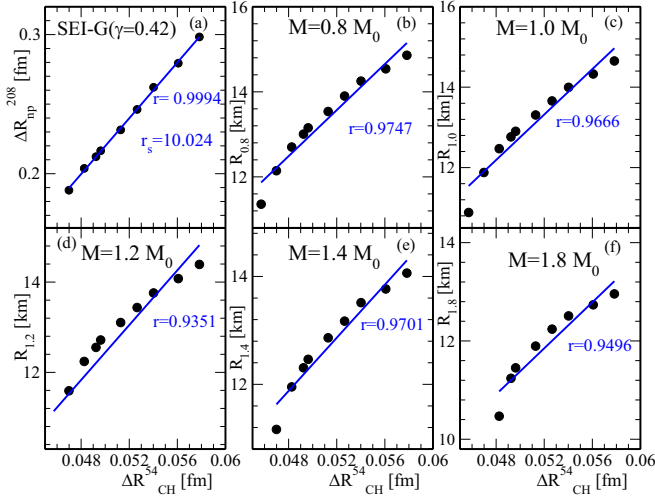


FIG. 4. Stellar radii for neutron stars having masses (b) $M = 0.8M_{\odot}$, (c) $1.0M_{\odot}$, (d) $1.2M_{\odot}$, (e) $1.4M_{\odot}$, and (f) $1.8M_{\odot}$ as a function of the charge radii difference $\Delta R_{\text{CH}}^{54}$ in the ^{54}Ni - ^{54}Fe mirror pair. The correlation coefficient r obtained from linear regression is given in each panel. The correlation between $\Delta R_{\text{CH}}^{54}$ and ΔR_{np}^{208} is shown in panel (a).

medium and heavy nuclei, but nature forbids by not providing their mirror pairs.

From the correlation between ΔR_{CH} and L shown in Fig. 2, we see that ΔR_{CH} increases with L . This increase in ΔR_{CH} for increasing L stems from the combined effect of Coulomb force and neutron pressure in nuclei. The pressure in pure neutron matter at saturation density ρ_0 is related to L as

$$P_N(\rho_0) \approx \frac{\rho_0 L}{3}. \quad (4)$$

On account of the Coulomb force, regardless of the L value of the EoS, the proton distribution is pushed out compared to the neutron distribution. Due to this, and taking into account the fit in Eqs. (2) and (3), we realize that the neutron skin ΔR_{np} has a small negative value when $\Delta R_{\text{CH}} = 0$. Thus, proton-rich nuclei in the isotopic and isotonic chains displayed in Fig. 1 have a negative neutron skin when computed with SEI. On the other hand, the nuclear surface is pushed out as L grows, owing to the increase in neutron pressure, as can be seen from Eq. (4), resulting in extension of the neutron (proton) distribution at the surface in neutron (proton) rich nuclei. Whether it is a finite nucleus or a neutron star, both systems are governed by the same strong interactions and the EoS relating pressure to density [18,70–73]; in a nucleus the neutron pressure acts against the nuclear surface tension, whereas in a NS it acts against gravity. Hence, the neutron skin thickness and the NS radius have a correspondence in the context of the L dependence, in spite of their very different size.

The correlation between the skin thickness ΔR_{np}^{208} in the ^{208}Pb nucleus and the radius of neutron stars was investigated in Refs. [74,75]. SEI calculations show that the charge radii difference $\Delta R_{\text{CH}}^{54}$ in the mirror pair ^{54}Ni - ^{54}Fe is strongly correlated to ΔR_{np}^{208} , as can be seen in panel (a) of Fig. 4, with correlation coefficient 0.9994 and regression slope $r_s =$

10.02. Due to the high accuracy reached in the measurement of $\Delta R_{\text{CH}}^{54}$ [9], this quantity seems an interesting candidate for correlating with different properties of stellar objects as an alternative to the skin thickness of ^{208}Pb , which presently has a larger uncertainty depending on the nature of the experiment performed to determine it. Keeping this in view, we have analyzed the behavior of the stellar radius R_{NS} of NSs having masses from $0.8M_{\odot}$ to $1.8M_{\odot}$ as a function of $\Delta R_{\text{CH}}^{54}$, obtained from the SEI EoSs with different slope parameter L . The results are shown in panels (b)–(f) of Fig. 4. In solving the TOV equations we have used the BPS-BBP EOS [76,77] up to a density 0.07468 fm^{-3} and the SEI EOS for densities thereafter. In each of these NSs of different masses, we find a linear correlation between the radius R_{NS} and the charge radii difference $\Delta R_{\text{CH}}^{54}$. When the mass of the NS grows, the quality of the linear fits shows a slight decreasing trend, which was first pointed out by Yang and Piekarewicz in Ref. [5]. In that work the correlation between the radius of low-mass NSs and the difference of proton radii in the mirror pair ^{50}Ni - ^{50}Ti was analyzed using well calibrated covariant EDFs covering a range of $L \approx 50$ – 140 MeV. The argument given in [5] for explaining this decreasing trend was that the slope parameter determines the EoS of neutron-rich matter around normal NM density and the central density of the low-mass NSs is relatively close to the NM saturation density, whereas heavier NSs have larger central densities. For the present SEI EoSs, the decrease in the quality of the correlation between R_{NS} and $\Delta R_{\text{CH}}^{54}$, from lighter to heavier NS masses, is found to be relatively moderate. The R_{NS} - $\Delta R_{\text{CH}}^{54}$ correlation in the $1.4M_{\odot}$ NS, displayed in panel (e) of Fig. 4, together with the data in panel (a) of this figure, confirm the correlation between $R_{1.4}$ and ΔR_{np}^{208} found in Ref. [21] for a set of well calibrated covariant EDFs. The NICER data analysis of the signals from the so far measured heaviest-mass pulsar PSR J0740+6620 [45], prescribes a limit on the radius of a $1.4M_{\odot}$ NS to be $R_{1.4} = 12.45 \pm 0.65$ km at 1σ level. Another different range, $R_{1.4} = 11.9 \pm 1.4$ km, was ascertained from the data analysis of the GW170817 event of a binary NS merger in Ref. [46] by the LIGO/VIRGO Collaboration. This result prescribes the upper limit to be 13.3 km, which is close to the 13.1 km value of the PSR J0740+6620 data. However, there is larger uncertainty in the lower limiting value, which is 10.5 km from the GW170817 data in comparison to 11.8 km from NICER PSR J0740+6620 data. From the R_{NS} - $\Delta R_{\text{CH}}^{54}$ correlation of Fig. 4(e) together with the $\Delta R_{\text{CH}}-L$ correlation in Fig. 2(d), we constrain the slope parameter L in the range ≈ 70 – 100 MeV from the NICER 1σ -level $R_{1.4}$ data of PSR J0740+6620. This range for L , though larger than the values extracted from theoretical studies [49,78–80] and from theoretical analyses of various experimental data [29,47,50,81,82], conforms to the range 106 ± 37 MeV obtained in Ref. [21] from the analysis of the PREX-2 data together with the L - ΔR_{np}^{208} correlation using a set of covariant EDFs. Also it is in good agreement with the range $70 \leq L \leq 101$ MeV extracted from the nucleon-nucleus elastic scattering cross section analyses of reactions involving isobaric analog states [52]. Our result also falls well within the range $42 \leq L \leq 117$ MeV estimated from the charged pion ratio measurement at high transverse momentum in neutron-rich Sn+Sn collisions [53], as well

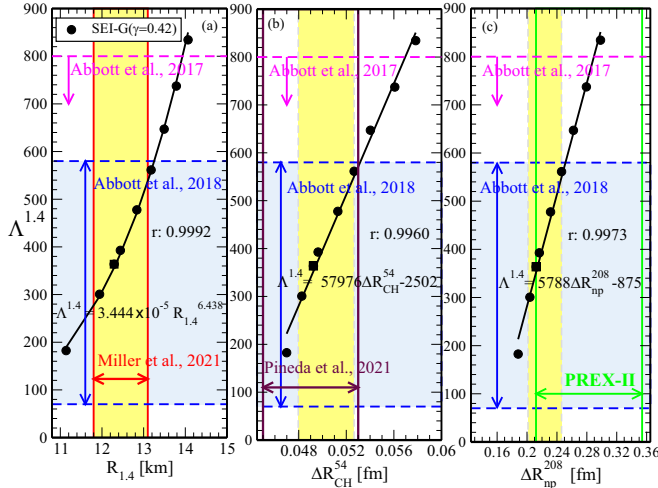


FIG. 5. Predictions of SEI-G ($\gamma = 0.42$) for the tidal deformability, $\Lambda^{1.4}$, in $1.4M_{\odot}$ NSs shown by filled black circles versus (a) the radius $R_{1.4}$ of $1.4M_{\odot}$ NSs, (b) charge radii difference ΔR_{CH}^{54} of the ^{54}Ni - ^{54}Fe mirror pair, and (c) neutron skin thickness ΔR_{np}^{208} in ^{208}Pb . The black squares correspond to the SEI calculation with characteristic slope parameter $L_C = 76.71$ MeV. The GW170817 2σ limits on $\Lambda^{1.4}$ [46] are shown between the blue horizontal lines and the earlier upper limit [84] by the pink line. In panel (a), the 1σ limits on $R_{1.4}$ from pulsar PSR J0740+6620 data [45] are shown by red vertical lines. In (b) the experimental data for ΔR_{CH}^{54} [9] are shown between maroon lines, and in (c) the PREX-2 limits [27] are shown by green vertical lines. In each panel the vertical yellow bands correspond to the SEI values in the range of $L = 70$ – 100 MeV for the respective variables $R_{1.4}$, ΔR_{CH}^{54} , and ΔR_{np}^{208} .

as within the range $63 \leq L \leq 113$ MeV ascertained from the transport model analysis of the isospin diffusion data [83].

The dimensionless tidal deformability parameter, $\Lambda^{1.4}$, for $1.4M_{\odot}$ NSs computed with SEI in the range $L = 70$ – 100 MeV is found to be compatible with the range $\Lambda^{1.4} = 190_{-120}^{+390}$ constrained from the analysis of the GW170817 data at 90% confidence 2σ level [46], which updates the previous upper limit of ≤ 800 [84]. In panels (a) and (b) of Fig. 5 we show by black filled circles the tidal deformability $\Lambda^{1.4}$ computed with SEI versus $R_{1.4}$ and ΔR_{CH}^{54} , respectively. Along the horizontal axis, in both panels, the $R_{1.4}$ and ΔR_{CH}^{54} values corresponding to the range of $L = 70$ – 100 MeV are shown by the vertical yellow bands. The $\Lambda^{1.4}$ values predicted by SEI within $L = 70$ – 100 MeV lie in a range of 300–560, which is within the constraint extracted from GW170817 [46] (shown between two horizontal lines in blue). We note that the NICER data for $R_{1.4}$ are at 1σ confidence, whereas the LIGO $\Lambda^{1.4}$ data are at 2σ -level accuracy. Thus, the inferences with regards to the $\Lambda^{1.4}$ constraint of GW170817 are subject to correction on the future availability of its data at 1σ confidence. We also see from panel (a) of Fig. 5 a strong power-law correlation between $\Lambda^{1.4}$ computed with SEI and $R_{1.4}$, which scales as $(R_{1.4})^{6.4}$ ([85] and references therein).

In order to estimate the degree of agreement of the SEI predictions with the PREX-2 data [27], we show in panel (c) of Fig. 5 the tidal deformability $\Lambda^{1.4}$ against the neutron

skin in ^{208}Pb . The SEI values of $\Delta R_{np}^{208} = 0.203$ – 0.246 fm in the range $L = 70$ – 100 MeV are shown by the vertical yellow band, and the PREX-2 data by two vertical green lines. As expected, a strong linear correlation between $\Lambda^{1.4}$ and ΔR_{np}^{208} is found. Although the upper limiting value $L = 100$ MeV can reproduce the PREX-2 data up to $\Delta R_{np}^{208} \approx 0.25$ fm, it fails in reproducing its central value 0.283 fm. However, ΔR_{np}^{208} predicted by SEI is compatible with the range 0.18 ± 0.07 fm found from the dispersive optical model analysis [86]. If we take as upper limit of $R_{1.4}$ the value 14.26 km from the NICER PSR J0030+0451 data [87], the PREX-2 result up to ≈ 0.31 fm can be explained, but in that case the tidal deformability constraint will be violated. The lower limiting value of the slope parameter $L = 70$ MeV satisfies the $\Lambda^{1.4}$ constraint and predicts $\Delta R_{np}^{208} = 0.20$ fm somewhat below the PREX-2 lower bound ($\Delta R_{np}^{208} = 0.212$ fm). This PREX-2 lower bound is predicted by the SEI EoS with the characteristic slope parameter $L_C = 76.71$ MeV. The recent CREX result for the neutron skin of ^{48}Ca , $\Delta R_{np}^{48} = 0.12 \pm 0.026(\text{exp}) \pm 0.024(\text{model})$ fm [28], indicates a softer EoS. Our calculations using SEI with L between 70 and 100 MeV predict ΔR_{np}^{48} in the range 0.175–0.195 fm, which is consistent with the model-averaged result $\Delta R_{np}^{48} = 0.176 \pm 0.018$ fm obtained in the EDF study in Ref. [14].

To examine the possibility of reproducing the CREX and PREX-2 data simultaneously within the present functional form of the SEI interaction, we have varied the basic nuclear matter properties of SEI without reference to the predictions of the EoS of $\gamma = 0.42$. Although a certain effect from the n - p effective mass splitting of SEI is found, the symmetry energy and its slope parameter have, as expected, the largest influence on the variation of the neutron skin thickness. By decreasing $E_s(\rho_0)$ and $L(\rho_0)$ to ≈ 30 and ≈ 20 MeV, respectively, the central value of the CREX data can be reproduced, but in that case ΔR_{np}^{208} gets substantially underestimated. If we increase $E_s(\rho_0)$ and $L(\rho_0)$ to reproduce the PREX-2 data, then ΔR_{np}^{48} gets much overestimated compared to CREX. The situation is reminiscent of the findings of the recent studies reported in Refs. [31,33]. In these works it was concluded that it is not possible to reproduce the CREX and PREX-2 data simultaneously with the present form of the nuclear EDFs. A similar situation is encountered in the chiral EFT calculations, where the *ab initio* theory predicts ΔR_{np}^{48} in the range of CREX [29], whereas the *ab initio* approach combined with recent advances in many-body techniques predicts ΔR_{np}^{208} in the range 0.12–0.22 fm [34]. This is consistent with the L value of the chiral EFT calculations, which lies in the range $L \approx 40$ – 60 MeV. In a separate work [32], the L - ΔR_{np}^{48} and L - ΔR_{np}^{208} correlations were analyzed using 207 EDFs. The authors of [32] find that two nonoverlapping ranges for L are required in order to predict ΔR_{np}^{48} and ΔR_{np}^{208} within the CREX and PREX-2 ranges, in agreement with the conclusions of Refs. [31,33].

IV. CONCLUSIONS

The isospin-symmetry breaking effect leading to a linear correlation between the proton rms radii difference in mirror

pairs and neutron skin thickness in nuclei, instead of equality between them, earlier found in the context of low-energy chiral EFT, Skyrme, and covariant functionals, is confirmed by calculations with the SEI finite-range model. The SEI model allows one to generate different parameter sets differing in their predictions in the isovector sector, which are characterized by the slope L of the symmetry energy, whereas the isoscalar properties remain invariant. We find that the available experimental data for charge radii differences in mirror nuclei pairs constrain L to the range ≤ 100 MeV. On the basis of the correlation found between the mirror pair charge radii difference and the NS radius, we have analyzed the radius of a NS of $1.4M_{\odot}$ as a function of the charge radii difference in the mirror nuclei ^{54}Ni and ^{54}Fe using the SEI model, since the $\Delta R_{\text{CH}}^{54}$ observable can be experimentally determined to high accuracy [9]. The $L \leq 100$ MeV limit extracted from the data of the charge radii differences in mirror nuclei pairs is found to be consistent with the $R_{1,4} = 12.45 \pm 0.65$ km radius constraint of the NICER data analysis for the pulsar PSR J0740+6620, which further constrains the slope parameter L in the range 70–100 MeV. In this range of L , the tidal deformability $\Lambda^{1.4} = 190_{-120}^{+390}$ extracted from the GW170817 event at 2σ level is well reproduced. In addition, the SEI model with L between 70 and 100 MeV explains the PREX-2 data on ΔR_{np}^{208} up to $\approx 30\%$ of the experimental range. But the CREX result

for ΔR_{np}^{48} is not reproduced, providing with $L = 70$ MeV a theoretical estimate at the upper limit ≈ 0.17 fm of the CREX value. This might be attributed to the inherent limitations in the functional form of the present NR and covariant EDFs discussed in Refs. [31,33]. In the context of PVES experiments, more precise electroweak measurements of the skin thickness of neutron-rich nuclei will be boosted by full operation of the future Mainz Energy-recovery Superconducting Accelerator (MESA) [88]. On the other hand, the continuing advances in laser spectroscopy may provide more data on charge radii along chains of mirror pairs, which can contribute to reducing the model dependence of the theoretical analyses and lead to new constraints on the properties of the isospin-dependent EoS.

ACKNOWLEDGMENTS

P.B. acknowledges support from MANF Fellowship of UGC, India. T.R.R. offers sincere thanks to Prof. B. Behera for useful discussions. M.C. and X.V. were partially supported by Grants No. PID2020-118758GB-I00 and No. CEX2019-000918-M (through the “Unit of Excellence María de Maeztu 2020-2023” award to ICCUB) from the Spanish MCIN/AEI [89].

-
- [1] X. F. Yang *et al.*, *Prog. Part. Nucl. Phys.* **129**, 104005 (2023).
- [2] P. Campbell, I. Moore, and M. Pearson, *Prog. Part. Nucl. Phys.* **86**, 127 (2016).
- [3] S. Malbrunot-Ettenauer, S. Kaufmann, S. Bacca, C. Barbieri, J. Billowes *et al.*, *Phys. Rev. Lett.* **128**, 022502 (2022).
- [4] B. A. Brown, *Phys. Rev. Lett.* **119**, 122502 (2017).
- [5] J. Yang and J. Piekarewicz, *Phys. Rev. C* **97**, 014314 (2018).
- [6] F. Sammarruca, *Front. Phys.* **6**, 90 (2018).
- [7] B. A. Brown, K. Minamisono, J. Piekarewicz *et al.*, *Phys. Rev. Res.* **2**, 022035(R) (2020).
- [8] M. Gaidarov, I. Moumene *et al.*, *Nucl. Phys. A* **1004**, 122061 (2020).
- [9] S. V. Pineda, K. König, D. M. Rossi, B. A. Brown *et al.*, *Phys. Rev. Lett.* **127**, 182503 (2021).
- [10] P.-G. Reinhard and W. Nazarewicz, *Phys. Rev. C* **105**, L021301 (2022).
- [11] S. J. Novario, D. Lonardonì, S. Gandolfi, and G. Hagen, *Phys. Rev. Lett.* **130**, 032501 (2023).
- [12] S. Abrahamyan, Z. Ahmed *et al.*, *Phys. Rev. Lett.* **108**, 112502 (2012).
- [13] A. Tamii, I. Poltoratska *et al.*, *Phys. Rev. Lett.* **107**, 062502 (2011).
- [14] J. Piekarewicz, B. K. Agrawal, G. Colò, W. Nazarewicz, N. Paar, P.-G. Reinhard, X. Roca-Maza, and D. Vretenar, *Phys. Rev. C* **85**, 041302(R) (2012).
- [15] D. M. Rossi, P. Adrich *et al.*, *Phys. Rev. Lett.* **111**, 242503 (2013).
- [16] B. Alex Brown, *Phys. Rev. Lett.* **85**, 5296 (2000).
- [17] P.-G. Reinhard and W. Nazarewicz, *Phys. Rev. C* **81**, 051303(R) (2010).
- [18] M. Thiel, C. Sfienti, J. Piekarewicz, C. J. Horowitz, and M. Vanderhaeghen, *J. Phys. G: Nucl. Part. Phys.* **46**, 093003 (2019).
- [19] J. Piekarewicz and F. J. Fattoyev, *Phys. Today* **72**(7), 30 (2019).
- [20] F. J. Fattoyev, J. Piekarewicz, and C. J. Horowitz, *Phys. Rev. Lett.* **120**, 172702 (2018).
- [21] B. T. Reed, F. J. Fattoyev, C. J. Horowitz, and J. Piekarewicz, *Phys. Rev. Lett.* **126**, 172503 (2021).
- [22] Y. Zhang, M. Liu, C.-J. Xia, Z. Li, and S. K. Biswal, *Phys. Rev. C* **101**, 034303 (2020).
- [23] H. Güven, K. Bozkurt, E. Khan, and J. Margueron, *Phys. Rev. C* **102**, 015805 (2020).
- [24] L. Baiotti, *Prog. Part. Nucl. Phys.* **109**, 103714 (2019).
- [25] M. Tsang, W. Lynch, P. Danielewicz, and C. Tsang, *Phys. Lett. B* **795**, 533 (2019).
- [26] M. Fasano, T. Abdelsalhin, A. Maselli, and V. Ferrari, *Phys. Rev. Lett.* **123**, 141101 (2019).
- [27] D. Adhikari *et al.*, *Phys. Rev. Lett.* **126**, 172502 (2021).
- [28] D. Adhikari, H. Albataineh *et al.*, *Phys. Rev. Lett.* **129**, 042501 (2022).
- [29] G. Hagen, A. Ekström, C. Forssén, G. R. Jansen, W. Nazarewicz *et al.*, *Nat. Phys.* **12**, 186 (2016).
- [30] J. Simonis, S. Bacca, and G. Hagen, *Eur. Phys. J. A* **55**, 241 (2019).
- [31] E. Yüksel and N. Paar, *Phys. Lett. B* **836**, 137622 (2023).
- [32] S. Tagami, T. Wakasa, and M. Yahiro, *Results Phys.* **43**, 106037 (2022).
- [33] P.-G. Reinhard, X. Roca-Maza, and W. Nazarewicz, *Phys. Rev. Lett.* **129**, 232501 (2022).
- [34] B. Hu, W. Jiang, T. Miyagi *et al.*, *Nat. Phys.* **18**, 1196 (2022).

- [35] B. Behera, T. R. Routray, and R. K. Satpathy, *J. Phys. G: Nucl. Part. Phys.* **24**, 2073 (1998).
- [36] B. Behera, X. Viñas *et al.*, *J. Phys. G: Nucl. Part. Phys.* **40**, 095105 (2013).
- [37] B. Behera, X. Viñas, T. R. Routray, and M. Centelles, *J. Phys. G: Nucl. Part. Phys.* **42**, 045103 (2015).
- [38] T. R. Routray, P. Bano, M. Anguiano, M. Centelles, X. Viñas, and L. M. Robledo, *Phys. Rev. C* **104**, L011302 (2021).
- [39] P. Bano, X. Viñas, T. R. Routray, M. Centelles, M. Anguiano, and L. M. Robledo, *Phys. Rev. C* **106**, 024313 (2022).
- [40] B. Behera, T. R. Routray, A. Pradhana, S. K. Patra, and P. K. Sahu, *Nucl. Phys. A* **794**, 132 (2007).
- [41] T. R. Routray, X. Viñas, D. N. Basu, S. P. Pattnaik, M. Centelles, L. M. Robledo, and B. Behera, *J. Phys. G: Nucl. Part. Phys.* **43**, 105101 (2016).
- [42] S. P. Pattnaik, T. R. Routray, X. Viñas, D. N. Basu, M. Centelles, K. Madhuri, and B. Behera, *J. Phys. G: Nucl. Part. Phys.* **45**, 055202 (2018).
- [43] C. Gonzalez-Boquera, M. Centelles, X. Viñas, and T. R. Routray, *Phys. Rev. C* **100**, 015806 (2019).
- [44] T. R. Routray, S. P. Pattnaik, C. Gonzalez-Boquera, X. Viñas, M. Centelles, and B. Behera, *Phys. Scr.* **96**, 045301 (2021).
- [45] M. C. Miller, F. K. Lamb *et al.*, *Astrophys. J. Lett.* **918**, L28 (2021).
- [46] B. P. Abbott *et al.* (Virgo and LIGO Scientific Collaborations), *Phys. Rev. Lett.* **121**, 161101 (2018).
- [47] X. Roca-Maza, X. Viñas, M. Centelles, B. K. Agrawal, G. Colò, N. Paar, J. Piekarewicz, and D. Vretenar, *Phys. Rev. C* **92**, 064304 (2015).
- [48] A. Klimkiewicz, N. Paar *et al.*, *Phys. Rev. C* **76**, 051603(R) (2007).
- [49] C. Drischler, R. J. Furnstahl, J. A. Melendez, and D. R. Phillips, *Phys. Rev. Lett.* **125**, 202702 (2020).
- [50] R. Essick, I. Tews, P. Landry, and A. Schwenk, *Phys. Rev. Lett.* **127**, 192701 (2021).
- [51] C. Y. Tsang, B. A. Brown, F. J. Fattoyev, W. G. Lynch, and M. B. Tsang, *Phys. Rev. C* **100**, 062801(R) (2019).
- [52] P. Danielewicz, P. Singh, and J. Lee, *Nucl. Phys. A* **958**, 147 (2017).
- [53] J. Estee, W. G. Lynch *et al.*, *Phys. Rev. Lett.* **126**, 162701 (2021).
- [54] U. C. Perera, A. V. Afanasjev, and P. Ring, *Phys. Rev. C* **104**, 064313 (2021).
- [55] A. Ong, J. C. Berengut, and V. V. Flambaum, *Phys. Rev. C* **82**, 014320 (2010).
- [56] B. Behera, T. R. Routray, and S. K. Tripathy, *J. Phys. G: Nucl. Part. Phys.* **36**, 125105 (2009).
- [57] F. Sammarruca, *Int. J. Mod. Phys. E* **19**, 1259 (2010).
- [58] R. B. Wiringa, *Phys. Rev. C* **38**, 2967 (1988).
- [59] A. Akmal, V. R. Pandharipande, and D. G. Ravenhall, *Phys. Rev. C* **58**, 1804 (1998).
- [60] V. B. Soubbotin and X. Viñas, *Nucl. Phys. A* **665**, 291 (2000).
- [61] V. B. Soubbotin, V. I. Tselyaev, and X. Viñas, *Phys. Rev. C* **67**, 014324 (2003).
- [62] M. Del Estal, M. Centelles, X. Viñas, and S. K. Patra, *Phys. Rev. C* **63**, 044321 (2001).
- [63] G. F. Bertsch and H. Esbensen, *Ann. Phys. (NY)* **209**, 327 (1991).
- [64] B. Behera, X. Viñas, T. R. Routray *et al.*, *J. Phys. G: Nucl. Part. Phys.* **43**, 045115 (2016).
- [65] Mass Explorer, DFT mass tables, available at <http://massexplorer.frib.msu.edu/content/DFTMassTables.html>
- [66] S. E. Agbemava, A. V. Afanasjev, D. Ray, and P. Ring, *Phys. Rev. C* **89**, 054320 (2014).
- [67] J.-P. Delaroche, M. Girod, J. Libert, H. Goutte, S. Hilaire, S. Péru, N. Pillet, and G. F. Bertsch, *Phys. Rev. C* **81**, 014303 (2010).
- [68] J. Birkhan, M. Miorrelli *et al.*, *Phys. Rev. Lett.* **118**, 252501 (2017).
- [69] M. Tanaka *et al.*, *Phys. Rev. Lett.* **124**, 102501 (2020).
- [70] S. J. Novario, G. Hagen, G. R. Jansen, and T. Papenbrock, *Phys. Rev. C* **102**, 051303(R) (2020).
- [71] H. Shen, F. Ji, J. Hu, and K. Sumiyoshi, *Astrophys. J.* **891**, 148 (2020).
- [72] C. Horowitz, *Ann. Phys.* **411**, 167992 (2019).
- [73] J. B. Wei, J. J. Lu, G. F. Burgio, Z. H. Li, and H. J. Schulze, *Eur. Phys. J. A* **56**, 63 (2020).
- [74] C. J. Horowitz and J. Piekarewicz, *Phys. Rev. C* **64**, 062802(R) (2001).
- [75] J. Carriere, C. J. Horowitz, and J. Piekarewicz, *Astrophys. J.* **593**, 463 (2003).
- [76] G. Baym, H. A. Bethe, and C. J. Pethick, *Nucl. Phys. A* **175**, 225 (1971).
- [77] G. Baym, C. J. Pethick, and P. Sutherland, *Astrophys. J.* **170**, 299 (1971).
- [78] K. Hebeler, J. Lattimer, C. Pethick, and A. Schwenk, *Astrophys. J.* **773**, 11 (2013).
- [79] A. W. Steiner and S. Gandolfi, *Phys. Rev. Lett.* **108**, 081102 (2012).
- [80] S. Gandolfi, J. Carlson *et al.*, *Eur. Phys. J. A* **50**, 10 (2014).
- [81] Z. Zhang and L.-W. Chen, *Phys. Lett. B* **726**, 234 (2013).
- [82] L.-W. Chen, C. M. Ko, B.-A. Li, and J. Xu, *Phys. Rev. C* **82**, 024321 (2010).
- [83] L. W. Chen, C. M. Ko, and B. A. Li, *Phys. Rev. C* **72**, 064309 (2005).
- [84] B. P. Abbott *et al.* (Virgo and LIGO Scientific Collaborations), *Phys. Rev. Lett.* **119**, 161101 (2017).
- [85] O. Lourenço *et al.*, *Phys. Lett. B* **803**, 135306 (2020).
- [86] C. D. Pruitt, R. J. Charity, L. G. Sobotka, M. C. Atkinson, and W. H. Dickhoff, *Phys. Rev. Lett.* **125**, 102501 (2020).
- [87] M. C. Miller *et al.*, *Astrophys. J.* **887**, L24 (2019).
- [88] D. Becker *et al.*, *Eur. Phys. J. A* **54**, 208 (2018).
- [89] <http://data.crossref.org/fundingdata/funder/10.13039/501100011033>.